

Optoacoustic microscopy based on pi-FBG ultrasound sensors

Georg Wissmeyer^{a,b,*†}, Rami Shnaiderman^{a,b,†}, Dominik Soliman^{a,b} and Vasilis Ntziachristos^{a,b}

^aInstitute of Biological and Medical Imaging (IBMI), Helmholtz Zentrum München, Neuherberg, Germany;
^bChair for Biological Imaging, Technische Universität München (TUM), Munich, Germany;

ABSTRACT

We present an optoacoustic (photoacoustic) microscopy (OAM) imaging system that uses a pi-shifted Fiber Bragg Grating (pi-FBG) as ultrasound (US) sensor. The sensor has an ultra-small footprint and hence allows for the detection of optoacoustic signals in close proximity to their origin. The interrogation of the pi-FBG is performed by a broadband pulsed laser, enabling a high sensitivity of the sensor as well as the elimination of ambient noise. We characterize the pi-FBG in terms of axial and lateral resolution as well as its bandwidth and find that its performance is comparable to US sensors that are based on the piezoelectric effect. We demonstrate the system's capabilities by images taken from *ex vivo* zebrafish and mouse ear samples. The results presented herein highlight that pi-FBGs are a promising tool for the comprehensive label-free optoacoustic imaging of biomedical samples.

Keywords: Optoacoustic microscopy; photoacoustic microscopy; interferometric detection of ultrasound; Fiber Bragg-Grating.

1. INTRODUCTION

Within the past decades, various new techniques have replaced or augmented classical optical microscopy in biological and medical applications. These techniques commonly aim at pushing the boundaries set by the highly diffusive nature of tissue. Confocal microscopy and two-photon/multiphoton microscopy pushed the penetration depth of diffraction-limited microscopy up to the millimeter scale but are eventually limited by optical diffusion in deep tissue as well ^{1,2}. Optoacoustic microscopy (OAM) circumvents this problem by not relying on the detection of back-scattered light. In this method, acoustic waves are generated by the absorption of short pulsed laser light in tissue. The following thermoelastic expansion in a specific voxel within the tissue creates acoustic waves that can be recorded by an ultrasound detector. In contrast to electromagnetic waves in the visible range, acoustic waves hardly suffer from scattering in tissue, hence allow precise spatial localization and imaging of light absorbing structures ³. As a consequence, optoacoustic imaging has had a big impact in the progress of biomedical imaging in the past decade ^{4,5}.

Commonly, optoacoustic methods utilize ultrasound sensors based on the piezoelectric effect. While these sensors have undergone decades of technological evolution, certain physical limitations apply to them, e.g. the technological challenge of manufacturing ultrathin layers of piezoelectric materials for efficient detection of high-frequency signals as well as the matching of acoustic impedances ^{6, 7}. Additionally, the physical size of such a sensor governs its performance, as the size of the active element is proportional to its sensitivity. As piezoelectric detectors are of a ferromagnetic or pyromagnetic nature, they are also prone to interfering noise caused by parasitic electromagnetic fields ⁸. As a consequence, piezoelectric detectors suffer from significant drawbacks in applications that require sensors with a small footprint or frameworks that include sources with strong electromagnetic interferences, e.g. in the emerging field of magnetoacoustic sensing of nanoparticles ⁹.

[†]These authors contributed equally to this work.

*georg.wissmeyer@tum.de.

Next to recent developments in silicon-based capacitive micro-machined ultrasonic transducers (CMUTs), which are limited by a narrow detection bandwidth¹⁰, a variety of methods have emerged that utilize all-optical approaches for the detection of ultrasound^{11,12}. In this work, we present an optical-resolution OAM system with a fiber-based pi-phase-shifted fiber Bragg grating (pi-FBG) as ultrasound detector. The interrogation system of this interferometry-based sensor is provided by coherence restoring pulsed interferometry (CRPI) and reveals promising results for biomedical applications.

2. METHODS

2.1 All-optical optoacoustic microscope

In **Fig. 1**, the experimental setup of our CRPI-based OAM system is presented. It can be divided into two separate elements: Firstly, the excitation part, generating acoustic signals within a given sample and secondly, the wideband pulsed interferometry system, detecting and recording the ultrasound signals.

For the excitation, a 515 nm DPSS laser (1.8 ns pulse width; Flare HP PQ Green 2 k-500, Innolight GmbH, Hannover, Germany) generates 570 μ J pulses at a repetition rate of 1.2 kHz. The beam is attenuated and passes through a telescopic system with a 25 μ m pinhole at the intermediate focal spot to filter the light spatially and to fill out the back aperture of the objective lens (PLN 10X, NA: 0.25, wd: 10.6 mm, Olympus, Hamburg, Germany). Here, the objective lens is mounted in a customized inverted microscope (AxioCam ICc 1, Zeiss, Jena, Germany). The microscope has a CCD camera to provide brightfield imaging (AxioCam ICc 1, Zeiss, Jena, Germany). The laser is then focused into the agar embedded samples which are placed in standard glass bottom petri dishes. The sample holder is integrated in a high-resolution piezoelectric *xyz*-stage set (*xy*-stage: MLS203-2; *z*-stage: ZMZS500-E; Thorlabs, Newton, New Jersey, USA).

The detection of ultrasound is based on the CRPI system presented in ref.¹³. For the interrogation of the pi-FBG, an

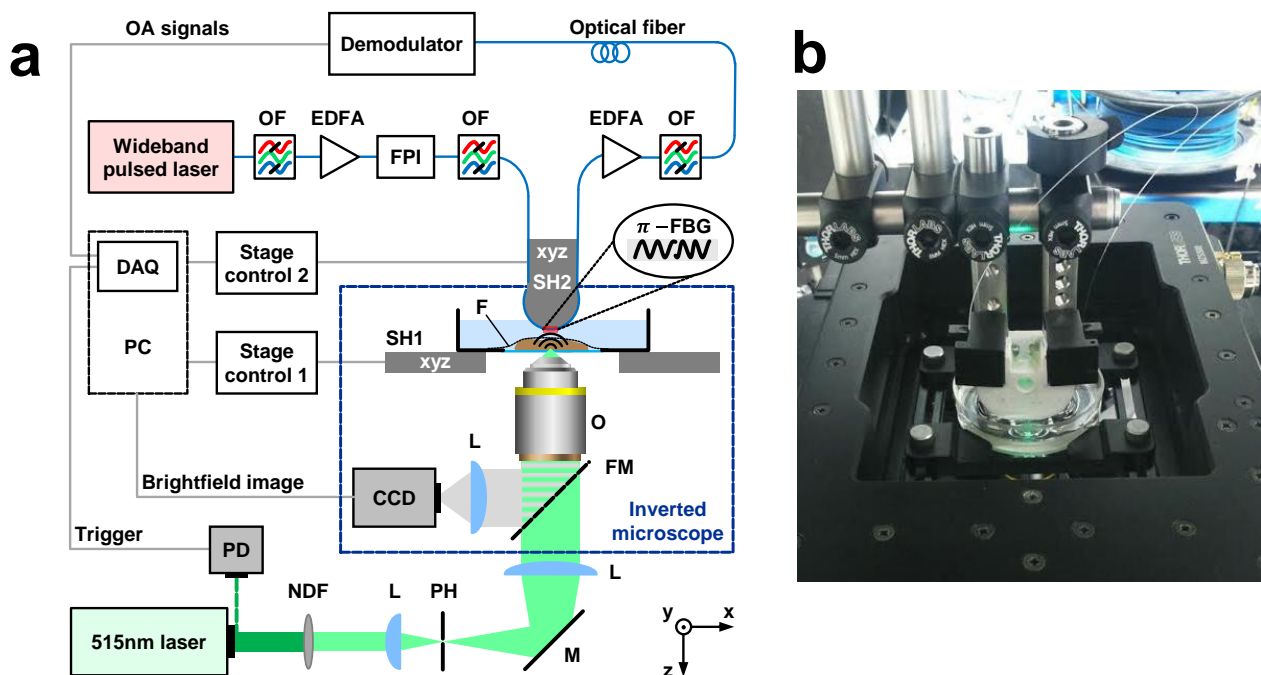


Figure 1: The all-optical optoacoustic microscope: (a) Schematic of the setup. OF, optical filter; EDFA, erbium-doped fiber amplifier; SH, sample holder; DAQ, data acquisition card; F, cover foil; O, microscope objective; PD, photodiode; NDF, neutral density filter; PH, pinhole; L, plano-convex lens; M, mirror; FM, flippable mirror. (b) Top-view of the sample holder and the fiber based sensor-head mounted on top of the inverted microscope. The pi-FBG is fixed onto the 3D-printed sensor-head (SH2) and then centered on top of the region of interest (SH1).

ultrafast femtosecond fiber laser with 1550 nm central wavelength and a pulse repetition rate of 1 GHz (Menlo Laser, TC-1550; Menlo Systems, Martinsried, Germany) is used. After a combined filtering to 0.4 nm bandwidth (tunable bandpass filter C-band, Optoplex Corp., Fremont, CA, USA) and subsequent amplification of the laser pulses (C-band EDFA optical fiber amplifier, Amonics Ltd., Hong Kong), the interrogation laser passes a Fabry-Pérot interferometer (FPI) (Optical Frequency Synthesizer, MenloSystems GmbH). The FPI rejects amplified spontaneous emission from the laser and locks the free spectral range to 250 MHz. This is achieved by a custom made feedback device driving the piezo-mirrors of the FPI¹⁴. The laser subsequently passes the pi-FBG where ultrasound induced perturbations on the resonator cause the notch to shift spectrally and proportional to the magnitude of the perturbation. After being both amplified in an EDF-Amplifier and filtered in bandwidth, the laser pulses are then passed to a balanced fiber-based Mach-Zehnder Interferometer (MZI). The MZI acts as a detector for the spectral shifts and allows the direct recording of detected ultrasound signals as voltage readout from the balanced photodiode. The sensor length of the pi-FBG is defined as the area over which the sensor exhibits >50% of its sensitivity and has a length of 270 μm for the presented system¹⁵. For the alignment of the pi-FBG relative to the beam focus, a custom 3D-printed sensor head is mounted on a xyz -stage set (xy -stage: PI M-683, z -stage: PI-M-501, Physik Instrumente, Karlsruhe, Germany). For the performed OAM measurements, the sample is then moved through the focus of the excitation beam in a raster-pattern. The devices in both system parts are driven by custom designed programs using MATLABTM and the following image processing is performed in MATLABTM and ImageJ.

2.2 Sensor characterization

The spectrum of pi-FBGs consists of a narrow transmission resonance (notch) in the center of a stop band. For the pi-FBG applied in this work, the transmission spectrum is shown in **Fig. 2a**. The measured bandwidth at -3 dB of the resonance was ~ 10 pm. Pi-FBGs exhibit sensitivity maps that are based on the cylindrical nature of the sensor as well as on orientation of the polarization maintaining fiber relative to the signal source¹⁶. **Fig. 2b** and **2c** show line scans of the pi-FBG across a stationary optoacoustic signal source. Such measurements are used to center the pi-FBG on top of the focused excitation beam and are found to be in good agreement with the theoretical effective detector length of ~ 300 μm ¹⁵.

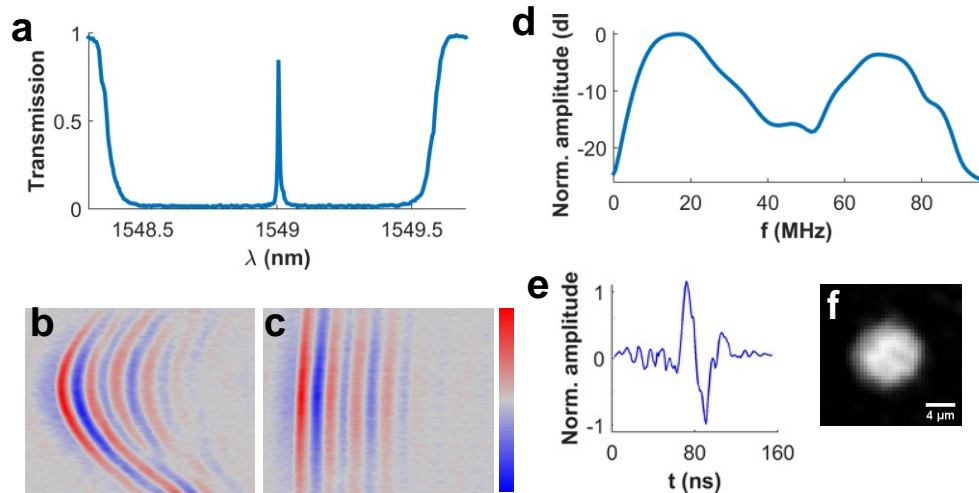


Figure 2: Characterization of the optical sensor: (a) Transmission spectrum of the pi-FBG. (b-c) Signals obtained for line scans of the sensor across a fixed optoacoustic source, with the scanning direction perpendicular (b) and parallel (c) to the geometrical axis of the pi-FBG. (d) Frequency response of the sensor to a black 10 μm polystyrene sphere. (e) Associated optoacoustic signal as recorded at a position near the center of the sphere. (f) OAM image of the microsphere.

The bandwidth of the system is defined as the frequency span over which the amplitude exceeds values of below -10 dB. From analyzing the Fourier transform of the time-domain signal, an overall bandwidth of 80 MHz was deduced as shown in **Fig. 2d**. Generally, the frequency response of the detector is governed by its cylindrical shape¹⁶ and the theoretical bandwidth of the CRPI system, which is limited to 125 MHz¹⁷. In the context of OAM, the lateral resolution of the presented system is governed by the optical resolution of the excitation setup, as the acoustic detector is of an unfocused nature. Hence, the lateral resolution is 2.2 μm , as experimentally determined in ref.¹⁸. In contrast, the axial resolution depends on the properties of the acoustic detector. Thus, we recorded the response of the pi-FBG sensor to optoacoustic signals generated by a black 10 μm diameter polystyrene sphere (Polybead, Polysciences, Warrington, USA). The time-domain signal at a position close to the center of the sphere is shown in **Fig. 2e** and the corresponding maximum intensity projection (MIP) is shown in **Fig. 2f**. The MIP was recorded with a step size of 0.5 μm . The axial resolution for optoacoustic signals is governed by the bandwidth of the sensor and was determined to be ~ 11 μm in accordance to ref.¹⁹.

3. RESULTS

3.1 Phantom imaging

In order to compare the performance of the applied pi-FBG to existing OAM setups, a suture phantom containing sutures with diameters of 10 μm , 20 μm and 30 μm (Dafilon Polyamide, B. Braun Melsungen AG, Melsungen, Germany), combined forming a triangle, was scanned with the OAM system using the pi-FBG and a 78 MHz spherically focused piezoelectric transducer (SONAXIS, Besancon, France) for comparison. The according MIPs are shown in **Fig. 3a** and **3b**, respectively, and were recorded with scanning step sizes of 5 μm . The comparison reveals a good SNR for the pi-FBG scan but also shows that noise in the interrogation system led to fluctuations in the detection sensitivity as indicated by inconsistencies and a degrading SNR in the right side of the MIP. Consequently, external sources causing noise and vibrations were kept to a minimum in the following experiments.

3.2 *Ex vivo* imaging

In the field of OAM, imaging of biomedical samples is commonly limited to thin specimens such as skin samples and small animals. As a result, zebrafish as well as mouse ears are common *ex vivo* models because of their thin nature as well as due to their delicate structures of their endogenous optical absorbers, which are melanocytes and hemoglobin, respectively. In our experiments, brightfield microscopy images were taken from the samples prior to recording the optoacoustic samples and the pulse energy of the excitation laser ranged from ~ 15 nJ to ~ 100 nJ. The step size for the performed mechanical sample scans was 5 μm .

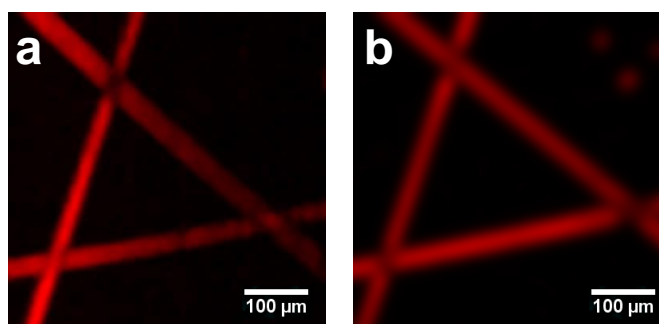


Figure 3: Optoacoustic images from a suture phantom. (a) MIP generated with signals recorded by the pi-FBG sensor. (b) MIP generated with signals recorded by a 78 MHz spherically focused piezoelectric transducer.

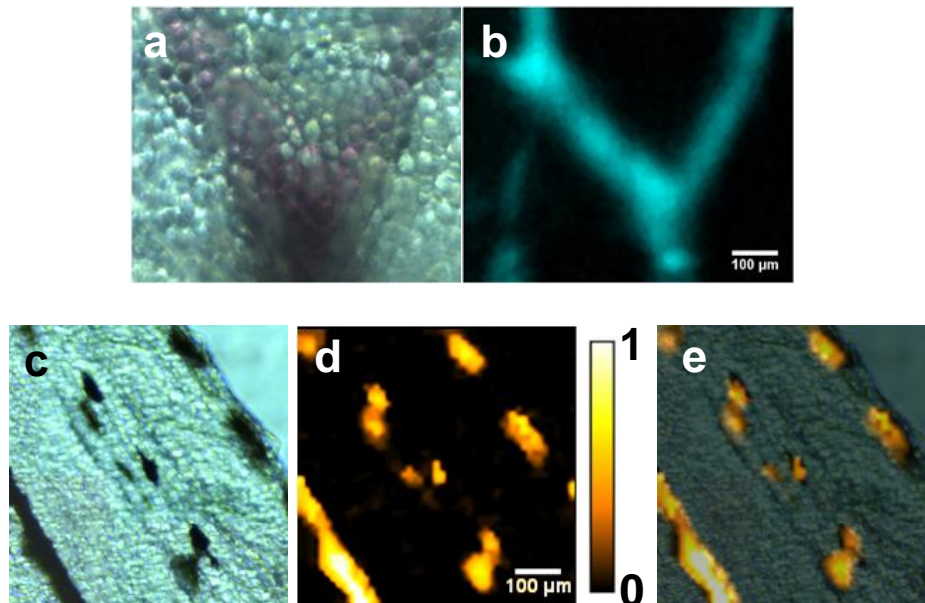


Figure 4: *Ex vivo* images of common OAM models. (a-b) Brightfield microscopy image and OAM MIP of a mouse ear, respectively, visualizing vasculature in the ear. (c-d) Brightfield microscopy image and OAM MIP of the back of a zebrafish larva, respectively, revealing melanophores. (e) Overlay of the brightfield image and the OAM MIP.

In the first experiment, an excised mouse ear (**Fig. 4a**) was embedded in a thin layer of centrifuged ultrasound gel and fixed by thin polyethylene foil in a glass bottom petri dish. The optoacoustic MIP of the same region of interest (**Fig. 4b**) reveals a Y-shaped structure in accordance to the vasculature that can be seen in the brightfield image. In addition, and most importantly though, the optoacoustic image further reveals thin vasculature as can be seen in lower the left part of the image and which is hidden in the brightfield image.

In the second experiment, a zebrafish larva was embedded in agar *ex vivo* and mounted onto the microscope in the same manner as the mouse ear specimen and initially imaged with the brightfield modality (**Fig. 4c**). The corresponding optoacoustic MIP using an excitation laser pulse power of 16 nJ is shown in **Fig. 4d** and the overlay of the brightfield and OAM images is presented in **Fig. 4e**. The overlay reveals an excellent matching between the two modalities. As can be observed, a good SNR was achieved with the all-optical OAM modality.

4. DISCUSSION AND CONCLUSIONS

In this work, we presented an all-optical optoacoustic microscope utilizing a pi-phase-shifted fiber Bragg grating as ultrasound detector. While theoretical values of sensitivity in terms of the noise equivalent pressure (NEP) have been shown and compared before^{17,18}, we for the first time showed and compared optoacoustic MIPs of the same sample recorded with a pi-FBG and a high-end piezoelectric US transducer. By this we were able to show that the sensitivity of pi-FBGs is on par with that of commonly embedded US detectors and that this technology is a promising technology for biomedical imaging. Furthermore, we demonstrated the applicability of pi-FBGs in OAM by the label-free imaging of

common model specimen *ex vivo*. Next to underlining the complementary contrast that is provided by OAM, the imaging of fine structures in a zebrafish larva revealed the high SNR of the detector even when using low laser excitation energy.

Generally, the ultra-small footprint of pi-FBGs may open the door for applications in setups that require sensors of ultra-small dimensions. Moreover, the immunity of such all-optical sensors against electromagnetic noise might allow for the application of OAM in new and emerging fields of biomedical imaging, as well as in non-destructive testing methods.

Due to the acoustic mismatch between the optical fiber and the coupling medium (e.g. water), the sensor could be further improved by using acoustically matching materials, e.g. polymers, or by applying pi-FBGs with higher Q-factors that would further increase the SNR of the system. Overall, the performance of the demonstrated ultrasound detector implemented in the optoacoustic microscope, along with its ultra-small dimensions, underline the potential to supplement or replace existing piezoelectric transducers.

Georg Wissmeyer acknowledges the support from the German Research Foundation (DFG) Research Grant (RO 4268/4-1).

5. REFERENCES

- [1] Yao, J., Wang, L. V., "Photoacoustic Microscopy," *Laser Phot. Rev* **7**(5), 1–36 (2014).
- [2] Ntziachristos, V., "Going deeper than microscopy: the optical imaging frontier in biology.," *Nat. Methods* **7**(8), 603–614, Nature Publishing Group (2010).
- [3] Chen, S., Guo, L. J., Wang, X., "All-optical photoacoustic microscopy," *Photoacoustics* **3**, 143–150, Elsevier GmbH. (2015).
- [4] Xu, M., Wang, L. V., "Photoacoustic imaging in biomedicine," *Rev. Sci. Instrum.* **77**(4), 1–22 (2006).
- [5] Jathoul, A. P., Laufer, J., Ogunlade, O., Treeby, B., Cox, B., Zhang, E., Johnson, P., Pizzey, A. R., Philip, B., et al., "Deep in vivo photoacoustic imaging of mammalian tissues using a tyrosinase-based genetic reporter," *Nat. Photonics* **9**(April), 239–246 (2015).
- [6] Xia, W., Piras, D., van Hespén, J. C. G., van Veldhoven, S., Prins, C., van Leeuwen, T. G., Steenberg, W., Manohar, S., "An optimized ultrasound detector for photoacoustic breast tomography," *Med. Phys.* **40**(3), 32901 (2013).
- [7] Small, D. M., Sanchez, W. Y., Hickey, M. J., Gobe, G. C., "Multiphoton fluorescence microscopy of the live kidney in health and disease Multiphoton fluorescence microscopy of the live kidney in health and disease," *J. Biomed. Opt.* **19**(2), 20901 (2014).
- [8] Rosenthal, A., Omar, M., Estrada, H., Kellnberger, S., Razansky, D., Ntziachristos, V., "Embedded ultrasound sensor in a silicon-on-insulator photonic platform," *Appl. Phys. Lett.* **104**(2) (2014).
- [9] Kellnberger, S., Rosenthal, A., Myklatun, A., Westmeyer, G. G., Sergiadis, G., Ntziachristos, V., "Magnetoacoustic Sensing of Magnetic Nanoparticles," *Phys. Rev. Lett.* **116**(10), 108103 (2016).
- [10] Rebling, J., Warshavski, O., Meynier, C., Razansky, D., "Optoacoustic characterization of broadband directivity patterns of capacitive micromachined ultrasonic transducers," *J. Biomed. Opt.* **22**(4), 41005 (2016).
- [11] Laufer, J., Zhang, E., Raivich, G., Beard, P., "Three-dimensional noninvasive imaging of the vasculature in the mouse brain using a high resolution photoacoustic scanner," *Appl. Opt.* **48**(10), D299 (2009).
- [12] Nuster, R., Holotta, M., Kremser, C., Grossauer, H., Burgholzer, P., Paltauf, G., "Photoacoustic microtomography using optical interferometric detection.," *J. Biomed. Opt.* **15**(2), 21307 (2010).
- [13] Rosenthal, A., Kellnberger, S., Bozhko, D., Chekkoury, A., Omar, M., Razansky, D., Ntziachristos, V.,

- “Sensitive interferometric detection of ultrasound for minimally invasive clinical imaging applications,” *Laser Photonics Rev.* **8**(3), 450–457 (2014).
- [14] Rosenthal, A., Kellnberger, S., Sergiadis, G., Ntziachristos, V., “Wideband Fiber-Interferometer Stabilization With Variable Phase,” *IEEE Photonics Technol. Lett.* **24**(17), 1499–1501 (2012).
- [15] Rosenthal, A., Caballero, M. Á. A., Kellnberger, S., Razansky, D., Ntziachristos, V., “Spatial characterization of the response of a silica optical fiber to wideband ultrasound,” *Opt. Lett.* **37**(15), 3174–3176, OSA (2012).
- [16] Veres, I. A., Burgholzer, P., Berer, T., Rosenthal, A., Wissmeyer, G., Ntziachristos, V., “Characterization of the spatio-temporal response of optical fiber sensors to incident spherical waves,” *J. Acoust. Soc. Am.* **135**(4), 1853–1862 (2014).
- [17] Rosenthal, A., Razansky, D., Ntziachristos, V., “Wideband optical sensing using pulse interferometry,” *Opt. Express* **20**(17), 19016 (2012).
- [18] Wissmeyer, G., Soliman, D., Shnaiderman, R., Rosenthal, A., Ntziachristos, V., “All-optical optoacoustic microscope based on wideband pulse interferometry,” *Opt. Lett.* **41**(9), 1953–1956 (2016).
- [19] Soliman, D., Tservelakis, G. J., Omar, M., Ntziachristos, V., “Combining microscopy with mesoscopy using optical and optoacoustic label-free modes,” *Sci. Rep.* **5**(August), 12902, Nature Publishing Group (2015).